Journal of Solid State Electrochemistry
https://doi.org/10.1007/s10008-024-05821-w

ORIGINAL PAPER

# Influence of active electrode impurity on memristive characteristics of ECM devices

Fabio Michieletti[1,2] · Shaochuan Chen[1] · Carsten Weber[3] · Carlo Ricciardi[2] · Takeo Ohno[4] · Ilia Valov[3,5]

Received: 14 November 2023 / Revised: 29 December 2023 / Accepted: 23 January 2024
© The Author(s) 2024

## Abstract

Memristive devices are promising candidates for the implementation in more than Moore applications. Their functionalities, electrical characteristics, and behavior, such as high scalability and stability at extreme conditions such as low/high temperatures, irradiation with electromagnetic waves and high-energy particles, and fast operation are required for solving current problems in neuromorphic architectures. Electrochemical metallization (ECM)-based memristive devices are among the most relevant in this scenario owing to their low power consumption, high switching speed, showing high HRS/LRS resistance ratio in digital mode, and as well multilevel to analogue-type performance, allowing to be used in wide spectrum of applications, including as artificial neurons and/or synapses in brain-inspired hardware. Despite all the advantages and progressing industrial implementation, effects of materials selection and interactions are not sufficiently explored, and reliable design rules based on materials approach are still to be formulated by the correct choice of structures and materials combinations to ensure desired performance. In this work, we report on the effects of impurities in the copper active electrode on the electrical characteristics of Cu/$Ta_2O_5$/Pt ECM devices. The results demonstrate that Cu impurity is modulating the electrochemical behavior and switching speed due to different catalytic activity and redox reaction rates. In addition, stability and variability are improved by decreasing the number of foreign atoms. Our results provide important additional information on the factors needed to be considered for rational device design.

## Introduction

Memristive devices have been demonstrated to be suitable for overcoming current technologies limitations in various fields of application, such as next generation non-volatile memories [1, 2], in-memory computing [3, 4], neuromorphic computing [5, 6], and room temperature metrology [7]. All these applications are enabled by the ability of memristors to store information through internal resistance modulation, which is capable of exhibiting binary and analog switching, synaptic and neuron functions [8, 9], fading memory [5], and discrete quantum effects [7]. Several classes of memristive devices were reported, where among all, these based on redox reactions [10], ferroelectric effect [11], magnetic field [12], and phase change materials [13] are considered most promising. Redox-based resistive devices include electrochemical metallization (ECM) devices, where redox reactions and cation transport play essential role and valence change mechanism (VCM) devices, where resistance change is based predominantly on anion motion, but cations can still be involved in the mechanism [14–16]. ECM devices

Fabio Michieletti and Shaochuan Chen contributed equally to this work.

✉ Takeo Ohno
takeo-ohno@oita-u.ac.jp

✉ Ilia Valov
i.valov@fz-juelich.de

1 Institute of Materials in Electrical Engineering 2 (IWE2), RWTH Aachen University, Sommerfeldstraße 24, 52074 Aachen, Germany

2 Department of Applied Science and Technology, Politecnico di Torino, C.so Duca degli Abruzzi 24, 10129 Torino, Italy

3 Peter Gruenberg Institute 7 (PGI7) and JARA-FIT, Research Centre Juelich, Wilhelm-Johnen-Straße, 52425 Juelich, Germany

4 Department of Engineering, Graduate School of Engineering, Oita University, Oita 870-1192, Japan

5 Institute of Electrochemistry and Energy Systems, Bulgarian Academy of Sciences, "Acad. G. Bonchev" str. N°10, 1113 Sofia, Bulgaria

Published online: 01 February 2024

show advantages in terms of scalability, HRS/LRS resistance ratio, multilevel switching, and low power consumption [17, 18]. The crucial challenge toward implementation in industrial applications of this class devices is the high functional variability induced by several intrinsic system factors such as the catalytic activity of the electrodes [19], the materials combination of the stack and capping layers [20], the strong electric field in the switching layer and related field accelerated reactions, and ion dynamics [21]. Nevertheless, extrinsic factors such as presence of impurities and/or moisture or protons in the stack can also influence the system properties and behavior [22–25]. Despite the fundamental understanding, research, and applications of memristive devices that are intensively progressing, several questions remain open. For instance, the influence of the impurities within the active electrode material on electrochemical processes and device functionalities have not been considered. The importance of the composition of the active electrode has been realized by Yeon et al. [26] revealing the strong influence of electrode composition on the resistive switching characteristics, showing that instead of using only Cu or Ag metal as active electrode, the use of Cu-Ag alloy with a proper Cu(Ag) concentration can improve not only device to device uniformity but also device stability and electrical performance. However, the concentration of doping/alloying phase was in the range of several percents. Luebben et al. [24] demonstrated that the presence of foreign components in $SiO_2$ switching layer even in ppm range can significantly modify the electric potential distribution within the nanodevice and thus influence resistive switching kinetics and performance.

In this work, we discuss the impact of impurities in the active electrode on the electrochemical processes and resistive switching characteristics in $Cu/Ta_2O_5/Pt$ ECM memristive devices. We performed cyclic voltammetry, *I–V* sweeps, and pulse measurements to study electrochemical behavior, resistive switching characteristics, stability, and SET kinetics. The results demonstrate an improvement in electrical stability and uniformity by using higher-purity Cu as active electrodes. Our results are of importance to improve the knowledge on the rational material–based design of ECM devices with optimal performance.

## Experimental details

The ECM cells (see cross-sectional view in Fig. 1a) were prepared on thermally oxidized one-inch $SiO_2/Si$ wafer. The 10-nm Ti and 30-nm Pt layers were deposited onto the substrate. The use of Ti helps to improve the adhesion between the Pt bottom electrode and the wafer. The $Ta_2O_5$ switching layer with a 10-nm thickness was deposited on bottom electrode Pt by radio frenquency (RF) reactive magnetron sputtering using a Ta target (99.5%). Optimized deposition parameters are 150 W of power, 0.04 mbar of pressure, 12 sccm of Ar flow, and 8 sccm of oxygen flow. The device area was defined by optical lithography and lift-off processes. A photoresist layer was spin-coated and patterned through UV photolithographic pattern transfer. Cu active electrode with a 30-nm thickness was sputtered by RF magnetron sputtering (at 10 W, 0.004 mbar, 15 sccm Ar flow sputtering condition) and covered with a 30-nm Pt capping layer (at 80 W, 0.005 mbar, 15 sccm Ar flow sputtering condition) to prevent Cu oxidation. The final top electrode patterns were obtained through acetone lift-off. The effect of active electrode impurity was studied by fabricating $Cu/Ta_2O_5/Pt$ samples in two classes, by varying Cu target purity: a 99.99% (4N) low-purity (LP) target (EVOCHEM), and a 99.9999% (6N) high-purity (HP) (JX Metals). The main impurities in the metal targets were provided by the producer as Ag, Al, As, Bi, Ca, Fe, S, Sb, Na, and K, with 70 ppm Ag. The individual impurities were not controlled, and their concentrations may vary within the defined total impurity ratio. Device configuration, active device area, and other compositional and layer deposition parameters were kept constant.

Electrical characterization and statistical analysis were performed on 13 low-purity samples and 25 high-purity samples with Pt bottom electrode grounded and electrical potentials applied to Cu top electrodes. All measurements were conducted at temperature 23 °C ± 3 °C and relative humidity 22% ± 4% on devices with $25 \times 25$-$\mu m^2$ area. Keithley 6430 source meter was used for cyclic voltammetry and *I–V* sweep measurements (Fig. 1b). Pulse measurements were conducted by using a Wavetek 395 waveform generator and current responses were read by a DPO 7254C oscilloscope. Redox reactions were investigated with pristine devices through cyclic voltammetry (CV). The voltage range during CV sweeps was set from −2.1 V to 2.2 V to avoid electroforming process (first SET), otherwise voltage swings from −2.9 V to 2.9 V. In all cases, current range of the source-meter was set to 1.6 nA. For each sweep rate, three devices were measured for both high- and low-purity samples. For each sample, 30 devices were measured. After the cyclic voltammetry, electrical characteristics under *I–V* sweepings were recorded. Current compliance during *I–V* sweep measurement was set to 1 mA for SET processes. Before starting the statistical analysis, 20 *I–V* cycles were performed for ensuring device stabilization. From successive cycles set voltage ($V_{SET}$), reset voltage ($V_{RESET}$), high resistive state (HRS), and low resistive state (LRS) were analyzed from the obtained IV curves. The HRS and LRS resistance were read at 0.2 V. Statistical approach was used by extracting quantiles of 60 IV curves, being the minimum observed population ensuring statistics convergence. For SET kinetics measurement, rectangular voltage pulses were applied to the top electrode with magnitudes of 0.7 V, 0.95 V, 1.2 V, 1.45 V, and 1.7 V (Fig. 3a). For each SET voltage, the measurement was repeated for 20 and

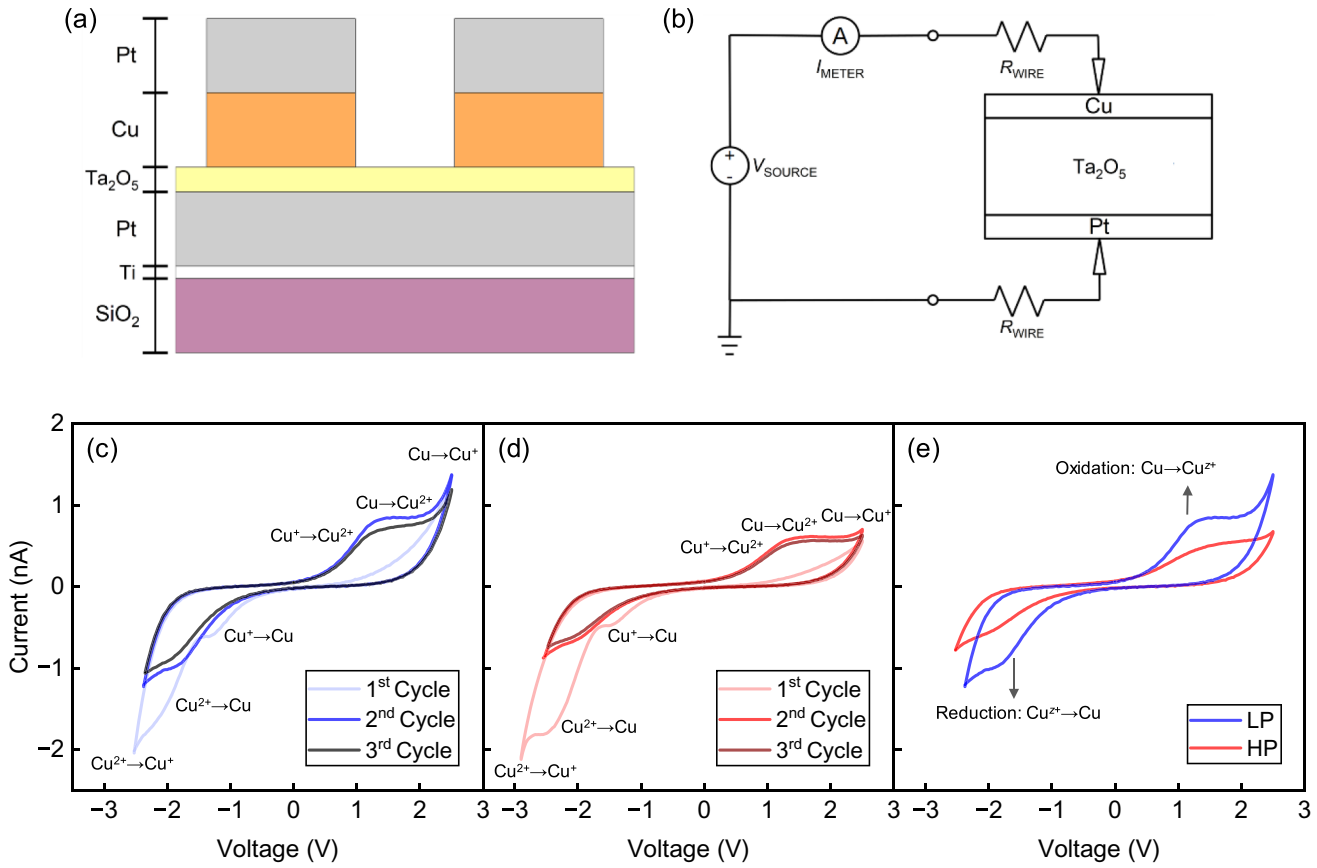



**Fig. 1** Schematics of **a** device structure and **b** the method for cyclic voltammetry and *I*–*V* sweep measurements. Exemplary cyclic voltammograms in low-purity device (**c**), high-purity device (**d**), and direct comparison of respective second cycles (**e**)

32 times and the SET time ($t_{SET}$) was acquired by calculating the time difference between the half rising edge of SET voltage pulse and SET current response.

## Results and discussion

Figure 1c, d, e shows exemplary cyclic voltammograms (CVs) for devices with low-purity (Fig. 1c) and high-purity (Fig. 1d) Cu electrode, with sweep rates of 370 mV/s. A direct compassion of current responses is shown in Fig. 1e. Both types of devices show pronounced redox current density peaks in the positive and negative voltage branch, indicating the oxidation of Cu active electrodes and reduction of Cu cations, respectively. The redox peaks observed on the CV correspond to different half-cell reactions of oxidation and reduction of Cu. We observed several redox steps during the complete sweep, characteristic for the reactions $Cu^{+} + e^{-} = Cu$; $Cu^{2+} + 2e^{-} = Cu$ and $Cu^{2+} + e^{-} = Cu^{+}$, respectively. The assignment of the peaks has been made, based on the standard electrode potentials in aqueous solutions. More detailed discussion on this can be found in reference [27]. Low-purity devices show higher redox currents, which is explained by the higher electrocatalytic activity of the electrodes due to impurity inclusions, leading to accelerated redox reaction rates. The origin of the higher reaction rate observed for low-purity metal can be twofold—more noble metal inclusions in Cu (e.g., Ag or Au) could form local galvanic elements that will increase the rate of dissolution of Cu, thus leading to faster SET process. In addition, less noble impurities such as Na, K, and Al can also be dissolved, serving as local donors, and higher concentrations will result in faster enrichment, and therefore faster kinetics. Based on our experiments, it is difficult to say at that stage whether both effects contribute equally, or one dominates. The voltage positions of the redox peaks for both reduction and oxidation processes show dependence on the Cu active electrode impurity, indicating a charge transfer limited processes. On the other hand, the current peak intensity also depends on the Cu active electrode impurity. Overall, the low-purity devices exhibit higher redox currents, more intensive redox current density peaks at lower voltage sweep potentials (Fig. 1e). Therefore, it is concluded that the presence of impurities in the electrodes is increasing

the catalytic activity of the electrodes towards the electrochemical processes, preceding the resistive switching, minimizing the charge transfer resistance. In the case of SET process, impurities are supposed to influence mainly the oxidation/dissolution of a Cu active electrode. However, during RESET, the parallel reaction of reduction of $H_2O$ molecules can also be affected by the impurities.

SET and RESET transitions were studied and compared for both systems by examining the *I–V* characteristics on multiple individual devices but as well in means of cumulative distributions for low-purity and high-purity devices. The analysis of the variability was obtained by evaluating the statistical distribution of individual device and by comparing the cumulative distribution of all devices. The statistical distribution of SET and RESET voltages can be better fitted to lognormal distribution (Fig. 2a, b). The fitting of HRS and LRS resistances were performed on logarithm values [17, 28]. The statistical distributions of $V_{SET}$, $V_{RESET}$, HRS, and LRS resistance values are depicted in Fig. 2. The upper panels in Fig. 2a–d show the device-to-device variation, whereas the bottom panels show the cumulative distribution. It can be observed that percentual variability (5–95%) is always significantly lower in high-purity copper devices. Furthermore, absolute variations are always greater in low-purity devices due to the broader distribution curves, particularly in the analysis of SET, RESET voltages, and HRS resistance. As reported by Celano et al. [29], formation of multiple filaments with different morphology, which alternately shortcuts the electrodes in different cycles, is a basis phenomenon influencing the switching variability. The presence of impurities may lead to different morphology and thickness variations between filaments (due to different local electrochemical activity). This effect would alter stochasticity and stability of the formed metallic filaments, causing an increase of the switching variability. Regarding measured resistances, we assume that compositional/thickness variation would cause an additional resistivity difference between the filaments. The presence of impurities can also catalyze parallel redox processes—which introduces additional voltage variability, observed in our devices.

To further study the influence of active impurity in the memristive switching, pulse measurement was conducted to reveal the temporal current response under certain pulse voltages stress. The waveform generators sent defined pulse waveforms to the devices under test. The oscilloscope channel 1 (CH1) monitored the real voltage signals generated by the waveform generator; concurrently, the current signals were recorded by monitoring the voltages drops across the shunt resistors in channel 2 (CH2) and channel 3 (CH3) of the oscilloscope. Figure 3a shows the schematic of the experimental setup. Figure 3b shows exemplary resistive switching cycle in pulse mode. Under the applied SET

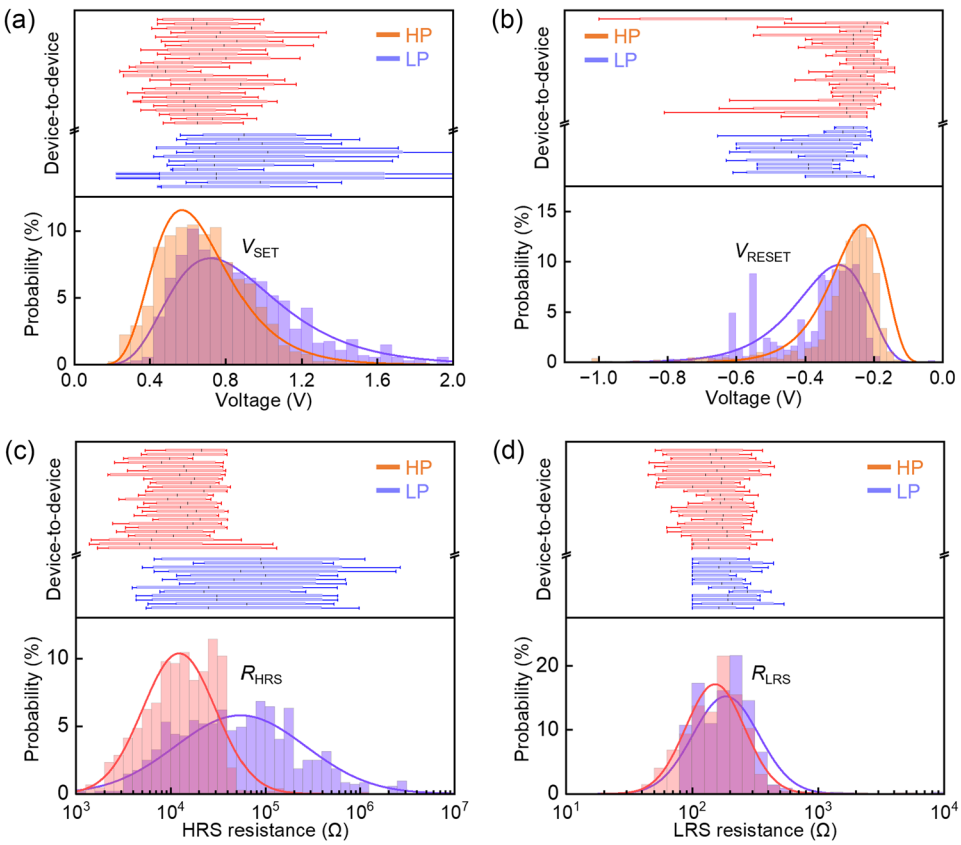



**Fig. 2** Influence of active electrode impurity on resistive switching characteristics. Comparisons of **a** SET voltage, **b** RESET voltage, **c** HRS resistance, and **d** LRS resistance. The box charts contain data in the range of 10 – 90%, the whiskers contain data in the range of 5 – 95%

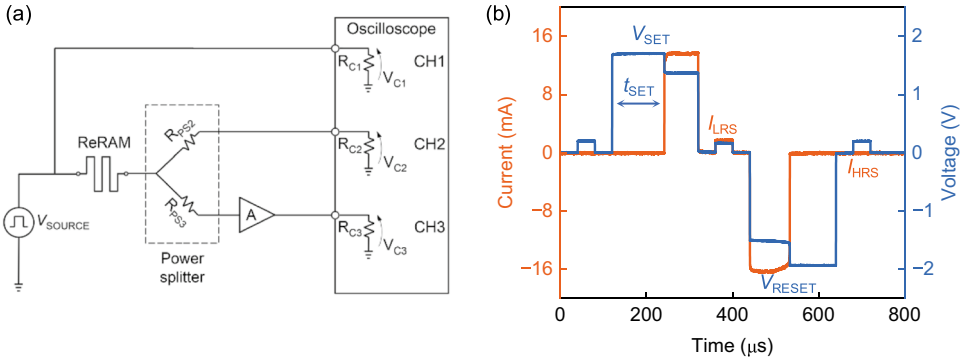



**Fig. 3** SET kinetics measurement (**a**) and transient current response under applied pulse voltage stress (**b**)

voltage ($V_{SET}$), the device switched from HRS to LRS after a time delay, after which the device current/conductance increase abruptly. The SET time is defined by the interval between the half rising edges of SET pulse and current response, as indicated in Fig. 3b. After each SET event, the device was switched back to HRS by the application of a RESET voltage pulse.

Figure 4a, b shows the SET time of devices with high- and low-purity electrodes as a function of applied voltage in pulse regime. Low-purity Cu devices demonstrate at each voltage faster switching, as shown in Fig. 4c. This result corresponds to the enhanced reaction rates observed in CV measurements (Fig. 1e). High-purity devices on the other side show higher stability and lower variability (Fig. 4b), consistent with the *I*–*V* sweep measurements (Fig. 2). We have further analyzed the SET kinetics presenting the pulse-mode data in $t_{SET}$ vs. *V* plots, following the model proposed by Menzel et al. [30]. In this model, three different regions are distinguished corresponding to nucleation, charge transfer, and diffusion limited processes. For our samples, only two regions were observed, and the fitted slopes are shown in Fig. 4a–c. We have excluded nucleation as a factor since it appears at much lower voltages and is characterized by much steeper slope. Thus, we associated the first region (0.7–1.2) V with charge transfer limitations. The kinetics confirms the observations on higher speed for low-purity

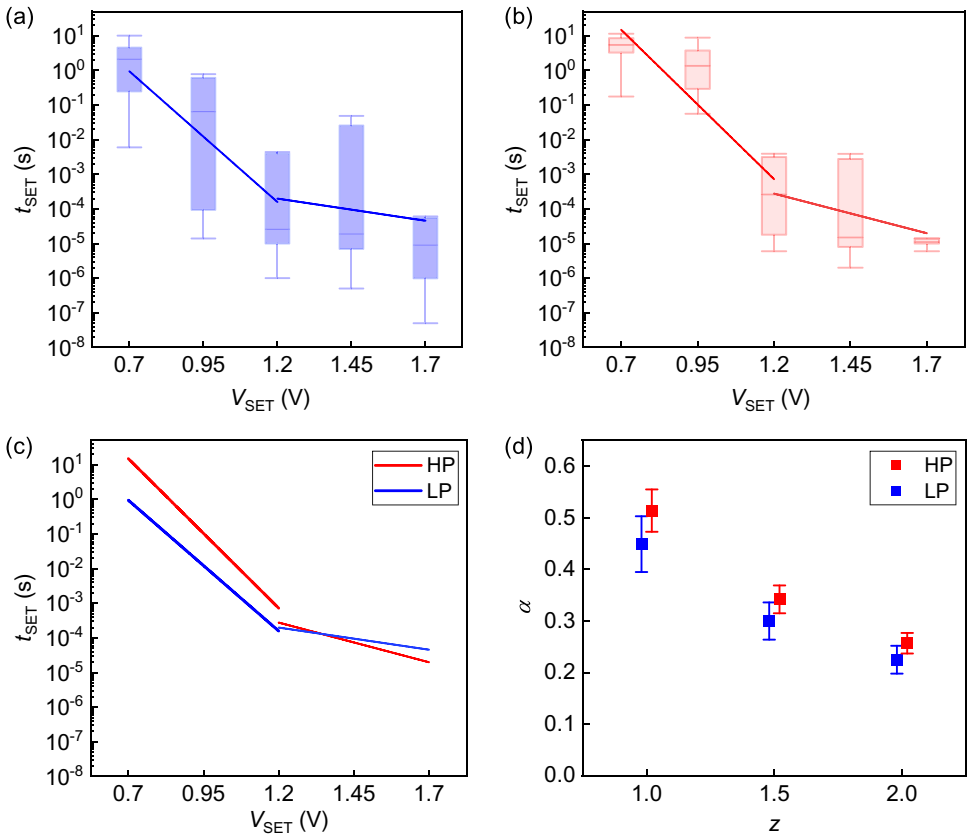



**Fig. 4** SET time distribution as a function of applied voltage for **a** low-purity and **b** high-purity samples. Solid lines report relative fittings for charge transfer limited and diffusion limited regions. Their comparison is shown in (**c**). In (**d**), extracted charge transfer coefficients are compared for $z = 1, 1.5, 2$

samples and lower slope $M_{RED}$, compared to high-purity electrodes. Using the dependence $M_{RED} = -\alpha ze/k_B T$, where $z$ is the number of transferred electrons, $e$ is the electron charge, $k_B$ is the Boltzmann constant, $T$ is the temperature. We have calculated the charge transfer coefficient $\alpha$, which is providing an information about the position of the energy barrier within the electric double layer. A challenge in determining of $\alpha$ is the uncertainty in defining the number of exchanged electrons $z$, related to the oxidation state of the Cu-ions in the oxide matrix. In previous studies, it has been shown that both $Cu^+$ and $Cu^{2+}$ can be present and participate in the reduction process [31].

Therefore, we have calculated and compared all three possibilities, i.e., $z = 1$, 1.5, and 2, respectively. $z = 1.5$ represents the case where statistically both 1 and 2 valence states are equally involved. As it can be seen from Fig. 4d, the charge transfer coefficient equals to ~ 0.5 for a single electron transfer reaction (corresponding to a barrier maximum situated in the middle of the double layer), which is the expected value. However, for $z = 2$, we obtain $\alpha \sim 0.22$, which also has been reported for other electrode reactions [32]. Therefore, despite the results indicate that reduced ions are $Cu^+$, the participation of $Cu^{2+}$ cannot be ruled out. On the effect of impurity concentration on $\alpha$ that can be speculated, Fig. 4 can be derived that low-purity samples have slightly lower transfer coefficient for all $z$. However, this conclusion needs additional confirmation. The second region observed in the $t_{SET}$ vs. $V$ plot at (1.2–1.7) V is associated with transport/diffusion limited processes. As clearly seen in Fig. 4, the difference between low- and high-purity samples is negligible and within the statistical error. Thus, we concluded that the purity of the electrodes is not playing a role for the switching at high-applied voltages.

The RESET kinetics also shows dependence on the purity of the metal electrodes; however, less pronounced. $V_{RESET}$ for high-purity Cu shows lower variability and lower voltages within the statistical evaluation (Fig. 2b). We interpret this effect as a result of the influence of impurity elements on the parallel redox reaction of $H_2O$ molecules, which is in this case competitive. Low-purity targets have higher reaction rate of the competitive reaction and therefore slower RESET kinetics. The RESET step is more complicated for analysis and evaluation of the kinetic parameters, as it also includes a thermally activated step, initially breaking the filament, followed by electrochemical dissolution.

## Conclusions

In this work, we reported the influence of impurities in the copper active electrodes on the electrochemical processes and following resistive switching performance in Cu/$Ta_2O_5$/Pt ECM memristive devices. Cyclic voltammograms, $I$–$V$ sweeps, and pulse measurement have demonstrated the even small number of foreign atoms in the electrode metal influence the redox reactions and switching characteristics and as well the LRS and HRS states. Cu electrodes with low-purity concentration show faster ionization/dissolution process than that of high-purity devices, resulting in faster kinetics and lower switching time. The electrode purity also is influencing the charge transfer at the electrode/electrolyte interface and the transfer coefficient. On the other hand, low-purity samples are characterized by higher switching variability. The reported results are providing knowledge on the additional factor of metal (im)purity that needs to be considered by materials choice, by designing memristive devices and targeting specific performance, such as for example stability and/or switching speed. This highlights the importance of continuing the studies on the effects impurities in metallic electrodes and expand these works to selective alloying with small amounts of foreign components/dopants. Our results are improving the current state-of-the-art knowledge on the effects of materials and material design of memristive devices on their characteristics and performance, contributing to better control and tuning the memristive properties in different applications.

**Acknowledgements** We acknowledge the Isohara Works of JX Metals for fabricating a high purity sputter target.

**Funding** Open Access funding enabled and organized by Projekt DEAL. This work has been funded in part by the project (EMPIR 20FUN06 MEMQuD) that has received funding from the EMPIR programme co-financed by the Participating States and from the European Union's Horizon 2020 research and innovation programme.

**Open Access** This article is licensed under a Creative Commons Attribution 4.0 International License, which permits use, sharing, adaptation, distribution and reproduction in any medium or format, as long as you give appropriate credit to the original author(s) and the source, provide a link to the Creative Commons licence, and indicate if changes were made. The images or other third party material in this article are included in the article's Creative Commons licence, unless indicated otherwise in a credit line to the material. If material is not included in the article's Creative Commons licence and your intended use is not permitted by statutory regulation or exceeds the permitted use, you will need to obtain permission directly from the copyright holder. To view a copy of this licence, visit http://creativecommons.org/licenses/by/4.0/.

## References

1. Golonzka O, Arslan U, Bai P, Bohr M, Baykan O, Chang Y, Chaudhari A, Chen A, Clarke J, Connor C, Das N, English C, Ghani T, Hamzaoglu F, Hentges P, Jain P, Jezewski C, Karpov I, Kothari H, Kotlyar R, Lin B, Metz M, Odonnell J, Ouellette D, Park J, Pirkle A, Quintero P, Seghete D, Sekhar M, Gupta AS, Seth M, Strutt N, Wiegand C, Yoo HJ, Fischer K (2019) Non-volatile RRAM embedded into 22FFL FinFET technology. IEEE Symposium on VLSI Technology (Kyoto, Japan: IEEE) pp T230–T231

2. Lee M-J, Lee CB, Lee D, Lee SR, Chang M, Hur JH, Kim Y-B, Kim C-J, Seo DH, Seo S, Chung U-I, Yoo I-K, Kim K (2011) A fast, high-endurance and scalable non-volatile memory device made from asymmetric Ta2O5−x/TaO2−x bilayer structures. Nat Mater 10:625–630
3. Mannocci P, Farronato M, Lepri N, Cattaneo L, Glukhov A, Sun Z, Ielmini D (2023) In-memory computing with emerging memory devices: status and outlook. APL Mach Learn 1:010902
4. Lelmini D, Wong H-SP (2018) In-memory computing with resistive switching devices. Nat Electron 1:333–343
5. Milano G, Pedretti G, Montano K, Ricci S, Hashemkhani S, Boarino L, Ielmini D, Ricciardi C (2022) In materia reservoir computing with a fully memristive architecture based on self-organizing nanowire networks. Nat Mater 21:195–202
6. Song M-K, Kang J-H, Zhang X, Ji W, Ascoli A, Messaris I, Demirkol AS, Dong B, Aggarwal S, Wan W, Hong S-M, Cardwell SG, Boybat I, Seo J, Lee J-S, Lanza M, Yeon H, Onen M, Li J, Yildiz B, del Alamo JA, Kim S, Choi S, Milano G, Ricciardi C, Alff L, Chai Y, Wang Z, Bhaskaran H, Hersam MC, Strukov D, Wong H-SP, Valov I, Gao B, Wu H, Tetzlaff R, Sebastian A, Lu W, Chua L, Yang JJ, Kim J (2023) Recent advances and future prospects for memristive materials, devices, and systems. ACS Nano 17:11994–12039
7. Milano G, Aono M, Boarino L, Celano U, Hasegawa T, Kozicki M, Majumdar S, Menghini M, Miranda E, Ricciardi C, Tappertzhofen S, Terabe K, Valov I (2022) Quantum conductance in memristive devices: fundamentals, developments, and applications. Adv Mater 34:2201248
8. Burr GW, Shelby RM, Sebastian A, Kim S, Kim S, Sidler S, Virwani K, Ishii M, Narayanan P, Fumarola A, Sanches LL, Boybat I, Gallo ML, Moon K, Woo J, Hwang H, Leblebici Y (2017) Neuromorphic computing using non-volatile memory. AdvPhys X 2:89–124
9. Chen S, Zhang T, Tappertzhofen S, Yang Y, Valov I (2023) Electrochemical-memristor-based artificial neurons and synapses—fundamentals, applications, and challenges. Adv Mater 35:2301924
10. Waser R, Dittmann R, Staikov G, Szot K (2009) Redox-based resistive switching memories – nanoionic mechanisms, prospects, and challenges. Adv Mater 21:2632–2663
11. Mikolajick T, Park MH, Begon-Lours L, Slesazeck S (2023) From ferroelectric material optimization to neuromorphic devices. Adv Mater 35:2206042
12. Parkin SSP, Roche KP, Samant MG, Rice PM, Beyers RB, Scheuerlein RE, O'Sullivan EJ, Brown SL, Bucchigano J, Abraham DW, Lu Y, Rooks M, Trouilloud PL, Wanner RA, Gallagher WJ (1999) Exchange-biased magnetic tunnel junctions and application to nonvolatile magnetic random access memory (invited). J Appl Phys 85:5828–5833
13. Koelmans WW, Sebastian A, Jonnalagadda VP, Krebs D, Dellmann L, Eleftheriou E (2015) Projected phase-change memory devices. Nat Commun 6:8181
14. Valov I, Waser R, Jameson JR, Kozicki MN (2011) Electrochemical metallization memories—fundamentals, applications, prospects. Nanotechnology 22:254003
15. Dittmann R, Menzel S, Waser R (2021) Nanoionic memristive phenomena in metal oxides: the valence change mechanism. Adv Phys 70:155–349
16. Wedig A, Luebben M, Cho D-Y, Moors M, Skaja K, Rana V, Hasegawa T, Adepalli KK, Yildiz B, Waser R, Valov I (2016) Nanoscale cation motion in TaO x, HfO x and TiO x memristive systems Nat. Nanotechnol 11:67–74
17. Kozicki MN, Barnaby HJ (2016) Conductive bridging random access memory—materials, devices and applications *Semicond*. Sci Technol 31:113001
18. Yoon JH, Zhang J, Lin P, Upadhyay N, Yan P, Liu Y, Xia Q, Yang JJ (2020) A low-current and analog memristor with Ru as mobile species. Adv Mater 32:1904599
19. Tappertzhofen S, Valov I, Tsuruoka T, Hasegawa T, Waser R, Aono M (2013) Generic relevance of counter charges for cation-based nanoscale resistive switching memories. ACS Nano 7:6396–6402
20. Chen S, Valov I (2022) Design of materials configuration for optimizing redox-based resistive switching memories. Adv Mater 34:2105022
21. Valov I, Lu DW (2016) Nanoscale electrochemistry using dielectric thin films as solid electrolytes. Nanoscale 8:13828–13837
22. Messerschmitt F, Kubicek M, Rupp JLM (2015) How does moisture affect the physical property of memristance for anionic–electronic resistive switching memories? Adv Funct Mater 25:5117–5125
23. Tsuruoka T, Terabe K, Hasegawa T, Valov I, Waser R, Aono M (2012) Effects of moisture on the switching characteristics of oxide-based, gapless-type atomic switches. Adv Funct Mater 22:70–77
24. Lübben M, Cüppers F, Mohr J, von Witzleben M, Breuer U, Waser R, Neumann C, Valov I (2020) Design of defect-chemical properties and device performance in memristive systems. Sci Adv 6:eaaz9079
25. Valov I, Tsuruoka T (2018) Effects of moisture and redox reactions in VCM and ECM resistive switching memories. J Phys Appl Phys 51:413001
26. Yeon H, Lin P, Choi C, Tan SH, Park Y, Lee D, Lee J, Xu F, Gao B, Wu H, Qian H, Nie Y, Kim S, Kim J (2020) Alloying conducting channels for reliable neuromorphic computing *Nat*. Nanotechnol 15:574–579
27. Tsuruoka T, Valov I, Tappertzhofen S, van den Hurk J, Hasegawa T, Waser R, Aono M (2015) Redox reactions at Cu, Ag/Ta2O5 interfaces and the effects of Ta2O5 film density on the forming process in atomic switch structures.AdvFunct Mater 25:6374–6381
28. Yu S, Ximeng G, Wong H-SP (2011) On the stochastic nature of resistive switching in metal oxide RRAM: physical modeling, monte carlo simulation, and experimental characterization. International Electron Devices Meeting (IEDM) (Washington, DC, USA: IEEE) pp 17.3.1–17.3.4
29. Celano U, Goux L, Belmonte A, Opsomer K, Detavernier C, Jurczak M, Vandervorst W (2015) Conductive filaments multiplicity as a variability factor in CBRAM. IEEE International Reliability Physics Symposium (IRPS) pp MY.11.1-MY.11.3
30. Menzel S, Tappertzhofen S, Waser R, Valov I (2013) Switching kinetics of electrochemical metallization memory cells *Phys*. Chem Chem Phys 15:6945–6952
31. Cho D-Y, Tappertzhofen S, Waser R, Valov I (2013) Bond nature of active metal ions in SiO2-based electrochemical metallization memory cells. Nanoscale 5:1781–1784
32. Valov I, Sapezanskaia I, Nayak A, Tsuruoka T, Bredow T, Hasegawa T, Staikov G, Aono M, Waser R (2012) Atomically controlled electrochemical nucleation at superionic solid electrolyte surfaces. Nat Mater 11:530–535


**Publisher's Note** Springer Nature remains neutral with regard to jurisdictional claims in published maps and institutional affiliations.